Solid State Ionics 268 (2014) 242–246

Contents lists available at ScienceDirect

Solid State Ionics

journal homepage: www.elsevier.com/locate/ssi

# Thermal stability of lithium-rich manganese-based cathode

Jan Geder [a,*], Jay Hyok Song [b], Sun Ho Kang [b], Denis Y.W. Yu [c,d,**]

[a] RP 2 — Energy Storage Systems, TUM CREATE, Singapore
[b] Energy1 Lab, Samsung SDI, Republic of Korea
[c] Energy Research Institute, Nanyang Technological University, Singapore
[d] School of Energy and Environment, City University of Hong Kong, Tat Chee Avenue, Kowloon, Hong Kong Special Administrative Region

ARTICLE INFO

*Article history:*
Received 27 July 2013
Received in revised form 21 May 2014
Accepted 31 May 2014
Available online 21 June 2014

*Keywords:*
Lithium-ion battery
Thermal stability
Lithium-rich layered oxide
$0.5Li_{4/3}Mn_{2/3}O_2$–$0.5LiNi_{1/3}Co_{1/3}Mn_{1/3}O_2$

ABSTRACT

Thermal stability of a lithium-rich layered oxide cathode material with composition $0.5Li_{4/3}Mn_{2/3}O_2$–$0.5LiNi_{1/3}Co_{1/3}Mn_{1/3}O_2$ (LMO–NCM) is investigated by thermogravimetric analysis (TGA) and differential scanning calorimetry (DSC). Investigated material shows higher thermal stability (higher onset temperature) than $LiCoO_2$. The state of charge and previous cycling history of LMO–NCM, particularly activation of lithium manganese oxide (LMO) "component" during first charge, affect its thermal stability. Activation of LMO has an ambivalent effect on cathode thermal stability: on the one hand, the onset temperature of cathode decomposition is increased, probably due to the change in oxidation states of Ni, Co and Mn after the first cycle. On the other hand, the enthalpy of decomposition increases, presumably due to formation of unstable oxygen in the lattice. X-ray diffraction (XRD) analyses of cathodes before and after thermal decomposition at 600 °C indicate differences in decomposition reactions of charged cathodes, depending on state of charge and cycling history.



## 1. Introduction

In lithium-ion battery, cathodes are usually considered as a limiting factor for efficient energy storage [1]. Most common cathode materials have low specific capacity, which equals approximately 130 to 150 mAh $g^{-1}$ for layered oxides $LiCoO_2$ (LCO) and $Li[Ni_{1/3}Co_{1/3}Mn_{1/3}]O_2$ (NCM), and 170 mAh $g^{-1}$ for $LiFePO_4$ (LFP) [2]. LCO is still the most commonly used cathode material for portable electronics due to its good balance between capacity, rate capability and ease of processing [3]. However, with increasing emphasis on safety of large-scale batteries, there is a need to develop alternative cathode materials with good thermal stability. Layered oxides LCO and NCM tend to decompose at higher temperatures, and the decomposition generates gaseous oxygen, which reacts with electrolyte, leading to thermal runaway of the cell [4]. Olivine LFP with good thermal stability has been proposed as a candidate to replace the layered oxides. However, it has a low packing density and it operates at low voltage, which leads to low energy density at cell level [3].

Lithium-rich layered oxides from the family $xLi_2MnO_3$-$(1-x)LiMO_2$ (M = Ni, Co, Mn), also known as LMO–NCM, have drawn much attention recently and are considered as alternative cathode materials [5]. Their advantages are high discharge capacity of more than 200 mAh $g^{-1}$ [6], and lower price due to lower Co content. On the other hand, main drawbacks of these materials are continuous voltage fade upon cycling, high irreversible capacity in first cycle and poor rate capability [5].

One special feature of these lithium-rich layered oxides is the characteristic charge profile during the first cycle that is different from that in the second cycle. Lithium is extracted separately from both components in the first cycle, resulting in two regions in the first charge curve: a first region up to 4.4 V where the NCM component is de-lithiated (i.e. increase in oxidation states of Ni and Co) and a second region above 4.4 V where the LMO component is activated [5]. Previous XANES experiments have suggested that the oxidation state of manganese in $Li_2MnO_3$ remains 4+ during charging, so the Li extraction is compensated by oxygen oxidation or oxygen gas release [6,7]. Phenomenologically, during discharge, most of the capacities can be accounted for by the reduction of Ni, Co and Mn transition metals in the material, with lithiation of the NCM component first above ~3.8 V and afterwards LMO below that. Thus, during the second charge, Li will be extracted first from the LMO component and then from the NCM component, resulting in a different charge profile as the first charge. We will show in the study that the difference in the first and second cycle charge mechanisms affects its thermal stability.

Recent research using differential electrochemical mass spectroscopy (DEMS) has confirmed $O_2$ gas release during first charge [8]. Further research suggests $O_2$ is released from the surface of the particles at the beginning of LMO activation plateau and oxygen is oxidized with

* Correspondence to: J. Geder, TUM CREATE, 1 CREATE Way, CREATE Tower #10-02, 138602, Singapore.
** Correspondence to: D.Y.W. Yu School of Energy and Environment, City University of Hong Kong, Tat Chee Avenue, Kowloon, Hong Kong.
*E-mail addresses:* jan.geder@tum-create.edu.sg (J. Geder), denisyu@cityu.edu.hk (D.Y.W. Yu).

http://dx.doi.org/10.1016/j.ssi.2014.05.020
0167-2738/

structure densification in the bulk at the end of the charging process [9,10]. Oxygen release and formation of unstable oxygen in the crystal structure of the active material raise additional concerns regarding material's safety.

This research aims to study the thermal stability of LMO–NCM based cathode and to compare it with conventional cathode materials such as LCO and NCM. Thermal stability of LMO–NCM is investigated as a function of state of charge (Li content) and cycling history. The influence of the LMO activation step (oxygen oxidation or gas emission) on thermal stability of material will be discussed.

## 2. Experimental

The active material was provided by Samsung SDI, Korea with a composition of $0.5Li_{4/3}Mn_{2/3}O_2$–$0.5LiNi_{1/3}Co_{1/3}Mn_{1/3}O_2$ (equivalent to $Li_{1.167}Mn_{0.5}Ni_{0.167}Co_{0.167}O_2$). Cathode slurry, composed of 80% active material, 10% acetylene black (AB; 50% compressed 99.9% metals basis, Alfa Aesar) and 10% polyvinylidene difluoride (PVdF, HSV900, Kynar) as 6% solution in N-Methyl-2-pyrrolidone (NMP; ACS reagent ≥99.0%, Sigma-Aldrich) was prepared and homogenized in a mortar and coated on a 15 μm Al foil with a doctor blade. The wet coating was dried on a hotplate at 80 °C. Rectangular cathodes (23 mm × 18 mm) were cut out and pressed several times in a roll press to obtain net electrode thickness of approximately 35 μm. The electrodes were then dried at 110 °C for 12 h in vacuum to remove any adsorbed water and transferred into an argon-filled glovebox, where pouch cells with pure metallic lithium as anode and 1 M $LiPF_6$ in 1:1 fluoroethylene carbonate/diethyl carbonate (FEC/DEC) as electrolyte were assembled. Each cell was cycled between 2.0 and 4.8 V with a current of 15 mA $g^{-1}_{LMO-NCM}$. Cells were charged to certain capacities in the first and in the second charge: the equivalent of 1st cycle irreversible capacity, 100 mAh, 150 mAh, 200 mAh, 250 mAh and 300 mAh per gram active material. Each charged cell was disassembled and the cathode was thoroughly washed with dimethyl carbonate (DMC; anhydrous, ≥99%, Sigma-Aldrich) and dried under vacuum for 12 h.

Charged, washed, and dried cathode materials were scratched off from the Al current collector, sealed into 100 μl Al crucibles by cold welding and thus prepared for thermal analysis. TGA and DSC were done simultaneously by MettlerToledo STARe TGA/DSC1 thermal analyzer. Crucible lid was pierced by the sampling robot before analysis in order to allow evolved gases to escape. Thermal analysis was conducted between 25 °C and 600 °C at a scan rate of 5 K $min^{-1}$ under a flow of argon (50 ml $min^{-1}$). After thermal analysis, samples were cooled down to 25 °C in the inert atmosphere under the same flow of argon.

For comparison, cathodes with same composition were prepared from NCM and LCO (both from Enax, Japan) as active materials. NCM cathodes were built into half-cells vs. Li using same electrolyte as for LMO–NCM and cycled between 2.75 and 4.8 V. NCM cathodes charged in both the first and second cycles were investigated to compare their cycling history dependence of thermal stability with that of LMO–NCM cathodes. LCO cathodes were built in half-cells vs. Li using 1 M $LiPF_6$ in 1:1 ethylene carbonate/diethyl carbonate (EC/DEC) as electrolyte and cycled between 3.0 and 4.2 V. Here the results of LCO cathode charged to 137 mAh $g^{-1}$ in the second cycle are reported. The same protocol of sample preparation was kept throughout for thermal analysis investigation.

All specific capacities in this paper are absolute. This means that the values refer to the cumulative capacity of the electrodes, i.e. the difference between total charge and discharge capacities starting from the beginning of cycling. We have assumed that no side reaction takes place during the charge–discharge process, so each electron passing the circuit is due to one lithium ion movement between the electrodes.

In order to investigate structural changes in the active material during charge/discharge and decomposition, powder X-ray diffraction (XRD) analysis was done by Rigaku SmartLab XRD in the range of $15° < 2\theta < 70°$ with Cu-Kα radiation (U = 45 kV, I = 100 mA). XRD measurements were repeated on the same samples before and after thermal treatment by TGA/DSC.

## 3. Results and discussion

### 3.1. Electrochemical characterization

Fig. 1 shows a characteristic cycling profile of the LMO–NCM cathode. During the first charge, the characteristic profile with two charging regions is observed. The first region below 4.4 V gives a charge capacity of about 154 mAh $g^{-1}$ (0.5 mol of Li removal), which is attributed to Li extraction from NCM component. The second region with a flat plateau at 4.5 V corresponds to the activation of LMO component. An overall charge capacity of 310 mAh $g^{-1}$ was achieved. During discharge, Li is inserted back into the lattice, in both the NCM component (at higher voltage) and the LMO component (at lower voltage). The first cycle discharge capacity was 255 mAh $g^{-1}$ with an irreversible capacity of 55 mAh $g^{-1}$. Multiple cells were made and charged and discharged to different states of charge (represented by squares in Fig. 1) for thermal stability tests. The cathode at different states of charge ($Li_{1.167-x}Mn_{0.5}Ni_{0.167}Co_{0.167}O_{2-y}$) from each cell was removed for the analysis. One should note that the electrodes with the same cumulative capacity (same amount of Li in the material) during the first and second charges have vastly different electrode potentials. This is unique for LMO–NCM and is not the case for LCO and NCM. This is due to the difference in the structure of the LMO–NCM material before and after LMO activation. Take for example samples (A) and (B) at a cumulative capacity of 150 mAh $g^{-1}$ during the first charge and second charge (x ~ 0.5), as indicated in Fig. 1. The open circuit potentials for the electrodes are 4.37 V and 3.28 V, respectively. Sample (A) has undergone first charging with Li removal only from the NCM component in the structure. The oxidation states of Ni, Co and Mn are in principle 4+. On the other hand, sample (B) has undergone LMO activation during first charge. Most of the charge–discharge capacity originates from oxidation state change of Mn below a potential of 3.8 V, and Ni and Co above 3.8 V. We expect sample (B) to have oxidation states of Ni and Co of close to 2+ and 3+, with a mixed oxidation state of Mn between 3+ and 4+. A comparison between the first and second cycles can therefore give us information on how the stability of the material is affected by the mechanism of LMO activation and the oxidation states of the transition metals in the material.

### 3.2. Thermal analysis

Fig. 2 shows TGA curves of the LMO–NMC cathodes in Ar at different states of charge. Dotted lines correspond to electrodes from the first

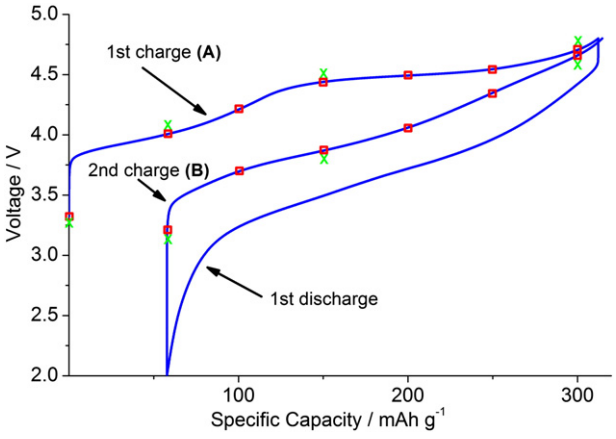


**Fig. 1.** Cycling profile of cathode vs Li between 2 and 4.8 V at a current of 15 mA $g^{-1}$. Squares indicate at which points cathodes were removed from the cells, washed, dried and analyzed by TGA/DSC. Crosses indicate at which points XRD spectra were taken for washed and dried cathodes, as well as thermally decomposed (after TGA/DSC) cathodes.

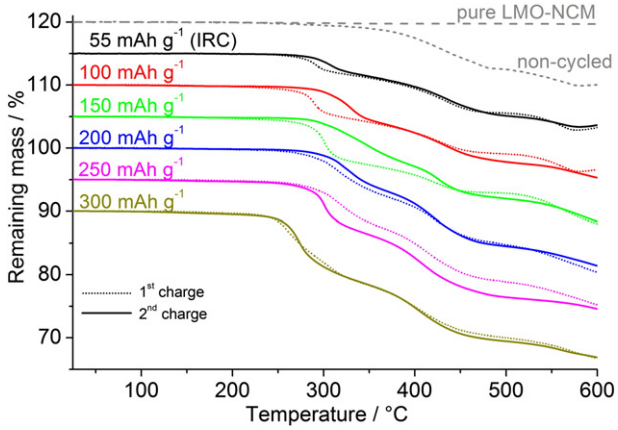


**Fig. 2.** TGA curves of pure LMO–NCM and charged, washed and dried LMO–NCM cathode at various states of charge in the 1st and 2nd cycles. Curves are shifted vertically by 5% each for purpose of clarity. Dotted lines correspond to electrodes from the first charge cycle and solid lines correspond to those from the second charge cycle. The dashed lines refer to as-received LMO–NCM active material and fresh electrode (blank) that is not tested electrochemically.

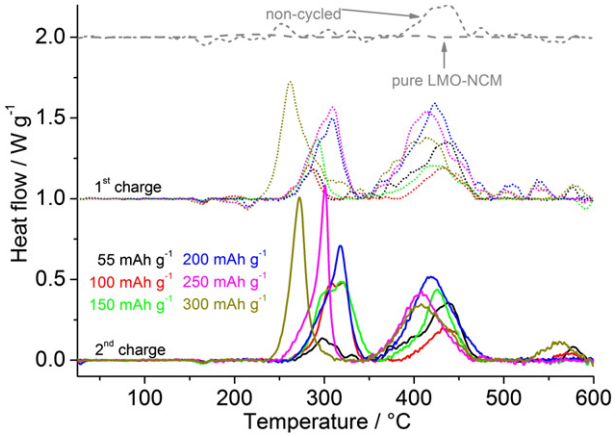


**Fig. 3.** DSC curves of LMO–NCM cathodes at different state of charge in the first (dotted line, shifted 1 W $g^{-1}$ for clarity) and second (solid line) cycle. The dashed lines refer to as-received LMO–NCM active material and fresh electrode (blank) that is not tested electrochemically.

charge cycle and solid lines correspond to those from the second charge cycle. The dashed lines refer to as-received LMO–NCM active material and fresh electrode (blank) that is not tested electrochemically. The TGA curves were shifted down by 5% each to make it easier to distinguish the differences in the profiles. The pure LMO–NCM powder (long dashed line) does not show any decomposition up to 600 °C. The blank electrode (short dashed line) contains binder and carbon black. The weight loss above 350 °C is due to the decomposition of the binder and also the reduction of the active material due to the presence of carbon. The charged electrodes show reduction of weight below 350 °C, which is attributed to the reduced stability of the Li-deficient active material. As expected, total mass loss increases with state of charge and the degree of Li removal, indicating large amount of decomposition for material with lower Li content.

For cathodes charged during the first charge (dotted lines), decomposition onset remains between 276 °C and 296 °C until 250 mAh $g^{-1}$, and decreases to 238 °C at 300 mAh $g^{-1}$. The onset temperature is typically an indication of how stable the structure of the material is. Based on the charging mechanism of LMO–NCM, we would expect a change in material structure after the activation of the LMO component above 153.7 mAh $g^{-1}$ However, the decrease in thermal stability (in terms of earlier decomposition onset) is only seen after 250 mAh $g^{-1}$, which is 100 mAh $g^{-1}$ above expected value. This coincides with recent findings of Koga et al. [9,10], who suggest the release of $O_2$ from the surface of particles at the beginning of LMO activation, and the oxidation of oxygen from the bulk at higher charge capacity. The decrease in onset temperature at a later part of charging is probably due to the formation of unstable oxidized oxygen in the material.

Fig. 3 shows the corresponding DSC curves of LMO–NCM cathode during decomposition. The first peak is related to active material decomposition, whereas the second peak is related to decomposition of the binder and the reduction of the active material by carbon black. The enthalpy (heat generated) of the active material decomposition is thus determined from the first exothermic peak. During the first charge cycle, enthalpy increases with increasing state of charge (see Table 1), which is reasonable because as more Li is extracted from the material, the energy released from the material is expected to increase during the thermal test.

The behaviors of the TGA and DSC results during the second charge cycle are different from those during the first charge cycle. First of all, comparing the electrodes with the same cumulative capacity (same amount of Li), the onset temperature for thermal decomposition during second charge is higher when the cumulative capacity is less than 200 mAh $g^{-1}$ (see Fig. 2 solid lines). This indicates that the material is thermally more stable during the second charge cycle even though the amount of Li in the material is the same. This is probably due to the difference in oxidation states of the transition metals in the material during the first and second charging: with higher oxidation states of Ni and Co in the sample during the first charge than the second charge. $Ni^{4+}$ and $Co^{4+}$ are not stable and will easily decompose with heat. When the cumulative capacity during the second cycle is >250 mAh $g^{-1}$, the decomposition onset temperature becomes lower, which is similar to that observed during the first charge cycle. This is probably because at a later part of charging during the second cycle, more of the Ni and Co are oxidized to 4+, lowering the stability of the material.

DSC results during the second charge cycle (see Fig. 3) show larger peaks than those during the first charge cycle. This means higher heat release during decomposition of these cathodes during the second charge cycle, even though they are thermally more stable in terms of onset temperature. We suspect the amount of heat release is mainly due to the unstable oxygen in the material from LMO activation during first charge. It may also be partly due to the oxidation state of the Mn. During the first charge cycle, Mn remains 4+. It is known that tetravalent Mn is a stable form of Mn in air. Therefore, during thermal decomposition, we expect no contribution to the enthalpy from Mn during the first cycle. On the other hand, during the first discharge, some of the Mn is converted to 3+. Therefore, during the second charge cycle, some heat will be generated from the $Mn^{3+}$ in the material.

In Fig. 4, TGA and DSC curves for cathodes with NCM and LCO as active material are presented. Contrary to LMO–NCM, NCM shows no significant dependence of thermal stability on previous cycle during initial two cycles. Decomposition onset temperatures of cathodes charged to 100, 150 and 200 mAh $g^{-1}$ remain around 320 °C with no significant changes between the first and second charges.

NCM shows better thermal stability than LMO–NCM. This may be due to lower BET surface area of NCM (about 0.2–0.5 $m^2$ $g^{-1}$) compared to LMO–NCM (about 3 $m^2$ $g^{-1}$), the absence of unstable oxygen and the

**Table 1**
Summarized TGA and DSC data for decomposition of LMO–NCM cathodes.

| | Onset temperature (TGA) | | Enthalpy (DSC, first peak) | |
|---|---|---|---|---|
| Charge capacity | 1st charge | 2nd charge | 1st charge | 2nd charge |
| 55 mAh $g^{-1}$ | 276 °C | 287 °C | 52 J $g^{-1}$ | 52 J $g^{-1}$ |
| 100 mAh $g^{-1}$ | 277 °C | 301 °C | 61 J $g^{-1}$ | 220 J $g^{-1}$ |
| 150 mAh $g^{-1}$ | 291 °C | 301 °C | 108 J $g^{-1}$ | 274 J $g^{-1}$ |
| 200 mAh $g^{-1}$ | 296 °C | 301 °C | 194 J $g^{-1}$ | 264 J $g^{-1}$ |
| 250 mAh $g^{-1}$ | 292 °C | 290 °C | 264 J $g^{-1}$ | 252 J $g^{-1}$ |
| 300 mAh $g^{-1}$ | 238 °C | 248 °C | 334 J $g^{-1}$ | 259 J $g^{-1}$ |

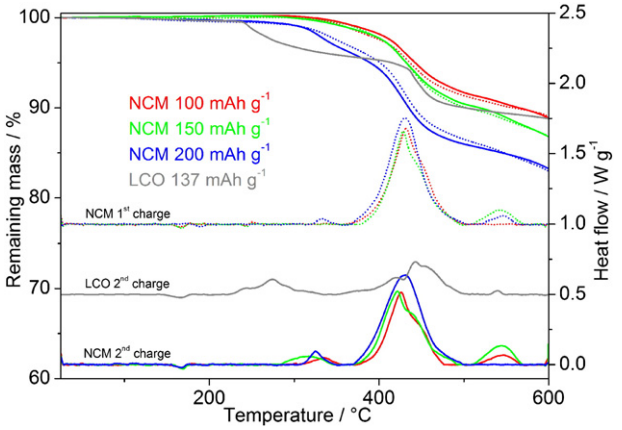


**Fig. 4.** TGA and DSC of reference electrodes with $Li[Ni_{1/3}Co_{1/3}Mn_{1/3}]O_2$ (NCM) and $LiCoO_2$ (LCO) as active material. Dotted line represents cathodes charged in the first cycle, and solid line represents cathodes charged in the second cycle. DSC curves are shifted 0.5 W $g^{-1}$ for clarity.

lower oxidation states of Ni and Co. Enthalpy during decomposition of NCM is not determined here because the decomposition of NCM thermally overlaps with decomposition of additives, forming one large peak in the DSC curves.

LMO–NCM, on the other hand, is more stable than LCO, which starts to decompose below 235 °C even when it is charged to 137 mAh $g^{-1}$ (0.5 Li removal).

### 3.3. X-ray diffraction analyses

To better understand the difference in the decomposition of cathodes between the first and second cycles, XRD was carried out before and after thermal decomposition on chosen cathodes. Spectra of received LMO–NCM material, dried non-cycled cathode, cathodes charged to 55 mAh $g^{-1}$ (equivalent to first cycle irreversible capacity), 150 mAh $g^{-1}$ (between both plateaus in first charge) and 300 mAh $g^{-1}$ (almost fully charged) in both the first and second cycles were taken.

Fig. 5 shows XRD of different samples before (a) and after (b) thermal treatment in TGA/DSC system. The XRD spectra of cathodes at various states of charge before thermal decomposition (Fig. 5a, left) show changes in crystal structure during the first cycle and subsequent charge. Most notable is the decrease of the relative intensity of the (003) peak between 18° and 19° during the first cycle and its consequent increase during the second charge. These changes reflect the activation of the material, in particular its LMO component, and are extensively described in references [9] and [11].

XRD spectra of decomposed cathodes are shown in Fig. 5b. The bottom figure shows the XRD profiles of the LMO–NCM powder and the fresh electrode after treatment in Ar to 600 °C. While there is no significant change in the XRD pattern for the LMO–NCM powder, the fresh electrode after thermal treatment shows completely different diffraction lines. This is due to reduction of the active material in the presence of carbon in the electrode. One of the prominent phases in all spectra after thermal treatment is the Fm-3m rock salt structure in the form of oxides with characteristic peaks at approximately 37°, 43° and 63°, which are most likely from the presence of $Co^{2+}$ and $Ni^{2+}$ or $Li_{0.5}Mn_{0.5}O_2$ from the reduction of the transition metal. The spectrum of the decomposed electrode charged to 300 mAh $g^{-1}$ shows additional peaks that most likely corresponds to $Mn_3O_4$ [12] and $LiMn_2O_4$, although MnO peaks are not observed.

The XRD patterns of the decomposed electrodes vary with state of charge (Li content). This is expected because the stable compounds after decomposition depend on Li content. It is interesting that the decomposition products also depend on the oxidation states of the transition metals, not only Li content. This can be verified by comparing the

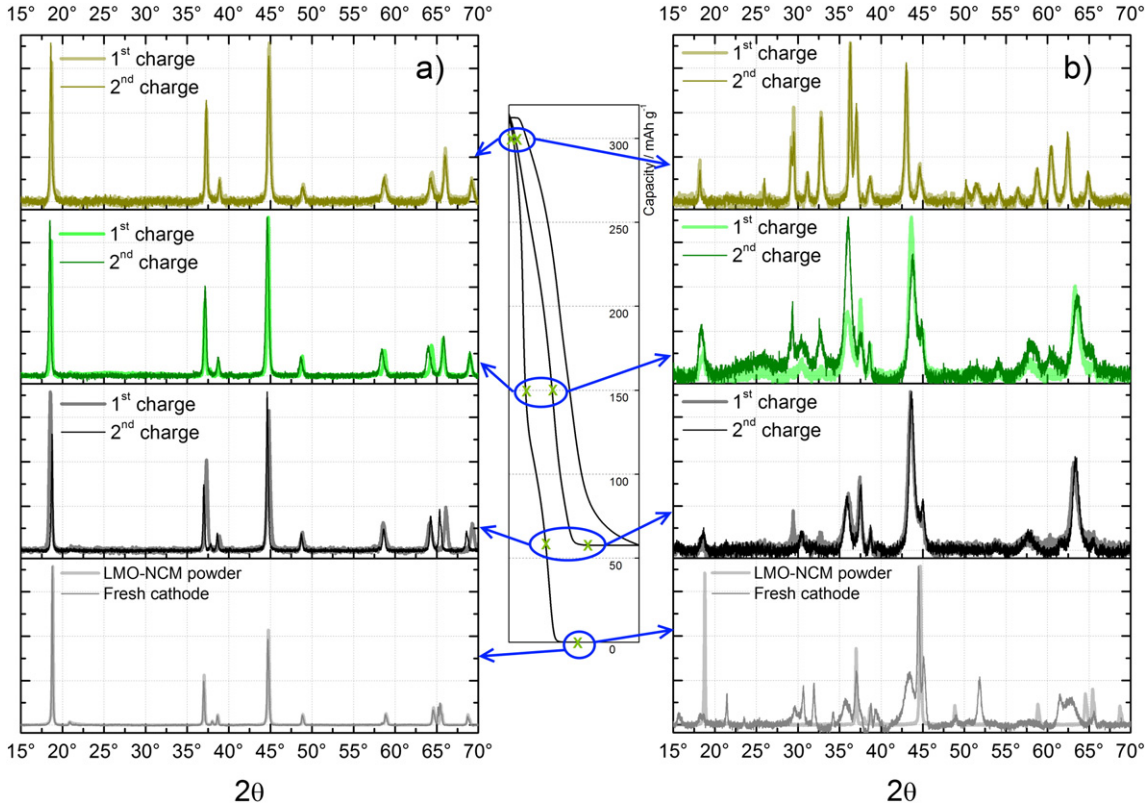


**Fig. 5.** XRD of pure as-received LMO–NCM and cathodes at various states of charge in the first and second cycles, before (a) and after (b) thermal decomposition in TGA–DSC. All spectra are normalized to the height of the highest peak in the respective spectrum.

XRD spectra of decomposed cathodes at the same state of charge in the first and second cycles. Spectra of decomposed fully charged cathodes at 300 mAh $g^{-1}$ show almost no difference between the first and second charges. The spectra of the decomposed cathodes at the equivalent of irreversible capacity (55 mAh $g^{-1}$) also show almost no differences, except for the peak at 29.5° which may be related to β-$MnO_2$-like structure [13]. On the other hand, the spectra of decomposed cathodes at 150 mAh $g^{-1}$ during the 1st and 2nd charges differ significantly, which is attributed to the difference in chemical environment of the two samples even though the Li content is the same. The actual oxidation states of the transition metals in the materials charged to 150 mAh $g^{-1}$ during the first and second cycles were not measured in this study, but we expect that they are vastly different, based on previous studies of other researchers [10]. In particular, the oxidation states of Ni, Co and Mn are expected to be close to 4+ for the electrode charged to 150 mAh $g^{-1}$ during the first cycle without the activation of the LMO component. For the cathode charged to 150 mAh $g^{-1}$ during the second cycle, the oxidation of Ni and Co are lower (probably 2+ and 3+) whereas that of Mn is between 3+ and 4+. These lead to different reaction products after thermal decomposition. It is therefore reasonable that the onset temperature and the enthalpy of the thermal decomposition are different depending on the history of the electrode, as discussed in the previous sections.

## 4. Conclusions

Thermal stability of lithium-rich manganese-based cathode active material (LMO–NCM) strongly depends on the activation of LMO component in the first cycle. During the first charge, thermal stability of the cathode is affected only above 250 mAh $g^{-1}$ charge. The probable cause is formation of unstable oxidized oxygen in the later stage of LMO activation. For electrodes with the same Li content, onset temperature of decomposition during the second charge cycle is in fact higher than that during the first. This could be due to difference in oxidation state of Ni, Co and Mn in the material during the first and the second charge–discharge.

Enthalpy of decomposition of the electrode is observed to increase during the first charge cycle with the amount of Li removal, whereas enthalpies are much higher during the second charge cycle. LMO–NCM is found to be thermally more stable than $LiCoO_2$ but less stable than $Li[Ni_{1/3}Co_{1/3}Mn_{1/3}]O_2$.

Overall, the amount of Li, amount of unstable oxygen, oxidation state of Ni, Co and Mn all contribute to the thermal stability of the LMO–NCM material, making it a very complicated system. XRD analyses show differences in products of thermal decomposition of cathodes with the same Li content before and after the first charge. This further confirms the influence of LMO component activation on thermal stability of the active material.

Further structural and calorimetric investigations of the material are undergoing to establish clear and distinct links between cycling-related structural changes and thermal stability as well as to elaborate influence of long-term cycling and cut-off voltage on thermal stability.

## Acknowledgments

This work was financially supported by the Singapore National Research Foundation under its Campus for Research Excellence And Technological Enterprise (CREATE) program.

## References

[1] S. Dou, J. Solid State Electrochem. 17 (2013) 911–926.
[2] M.S. Whittingham, Chem. Rev. 104 (2004) 4271–4301.
[3] H. Awano, in: M. Yoshio (Ed.), Springer Science + Business Media LLC, New York, 2009, pp. 300–301.
[4] D.D. MacNeil, J.R. Dahn, J. Electrochem. Soc. 148 (2001) A1205–A1210.
[5] H. Yu, H. Zhou, J. Phys. Chem. Lett. 4 (2013) 1268–1280.
[6] A. Ito, Y. Sato, T. Sanada, M. Hatano, H. Horie, Y. Ohsawa, J. Power Sources 196 (2001) 6828–6834.
[7] M. Oishi, et al., J. Power Sources 222 (2013) 45–51.
[8] P. Lanz, H. Sommer, M. Schulz-Dobrick, P. Novak, Electrochim. Acta 93 (2013) 114–119.
[9] H. Koga, L. Croguenec, M. Ménétrier, P. Mannessiez, F. Weill, C. Delmas, J. Power Sources 236 (2013) 250–258.
[10] H. Koga, L. Croguenec, M. Ménétrier, K. Douhill, S. Belin, L. Bourgeois, E. Suard, F. Weill, C. Delmas, J. Electrochem. Soc. 160 (2013) A786–A792.
[11] N. Yabuuchi, K. Yoshii, S.-T. Myung, I. Nakai, S. Komaba, J. Am. Chem. Soc. 133 (2011) 4401–4419.
[12] V. Baron, J. Gutzmer, H. Rundlof, R. Tellgren, Am. Mineral. 83 (1998) 786–793.
[13] J. Haines, J.M. Léger, S. Hoyau, J. Phys. Chem. Solids 56 (1995) 965–973.